Research Article

Nano Research
2020, 13(8): 2072–2078

ISSN 1998-0124 CN 11-5974/O4
https://doi.org/10.1007/s12274-020-2809-6

Direct bandgap engineering with local biaxial strain in few-layer MoS_2 bubbles

Yang Guo[1,2,§], Bin Li[3,§], Yuan Huang[1,§], Shuo Du[1,2], Chi Sun[1,2], Hailan Luo[1], Baoli Liu[1,2,4], Xingjiang Zhou[1], Jinlong Yang[3], Junjie Li[1,2,4], and Changzhi Gu[1,2] (✉)

[1] *Beijing National Laboratory for Condensed Matter Physics, Institute of Physics, Chinese Academy of Sciences, Beijing 100190, China*
[2] *School of Physical Sciences, CAS Key Laboratory of Vacuum Physics, University of Chinese Academy of Sciences, Beijing 100190, China*
[3] *Hefei National Laboratory for Physical Sciences at the Microscale and Synergetic Innovation Center of Quantum Information & Quantum Physics (CAS), University of Science and Technology of China, Hefei 230026, China*
[4] *Songshan Lake Materials Laboratory, Dongguan 523808, China*
[§] *Yang Guo, Bin Li, and Yuan Huang contributed equally to this work.*

Received: 23 December 2019 / **Revised:** 10 April 2020 / **Accepted:** 13 April 2020

ABSTRACT

Strain engineering provides an important strategy to modulate the optical and electrical properties of semiconductors for improving devices performance with mechanical force or thermal expansion difference. Here, we present the investigation of the local strain distribution over few-layer MoS_2 bubbles, by using scanning photoluminescence and Raman spectroscopies. We observe the obvious direct bandgap emissions with strain in the few-layer MoS_2 bubble and the strain-induced continuous energy shifts of both resonant excitons and vibrational modes from the edge of the MoS_2 bubble to the center (10 μm scale), associated with the oscillations resulted from the optical interference-induced temperature distribution. To understand these results, we perform *ab initio* simulations to calculate the electronic and vibrational properties of few-layer MoS_2 with biaxial tensile strain, based on density functional theory, finding good agreement with the experimental results. Our study suggests that local strain offers a convenient way to continuously tune the physical properties of a few-layer transition metal dichalcogenides (TMDs) semiconductor, and opens up new possibilities for band engineering within the 2D plane.

KEYWORDS

two-dimensional (2D) layered materials, transition metal dichalcogenides, band engineering, local strain

1 Introduction

Two-dimensional (2D) layered materials such as graphene and transition metal dichalcogenides (TMDs) possess fascinating properties for potential applications in novel spintronic and optoelectronic devices [1–5]. Unlike gapless graphene, TMDs are typical semiconductors with the energy gap in the near-infrared to visible spectral region and can be used for optoelectronic device applications such as photodetectors, solar cells and biosensors. TMDs consist of stacked X–M–X layers, with the chalcogen atoms (X = S, Se, Te) in two trigonal planes separated by a plane of metal atoms (M = Mo, W). Atoms within the X–M–X layer are bonded covalently, while individual sheets are bound via weak van der Waals interaction, which allow these materials to be easily thinned to single and few-layers via mechanical and chemical exfoliation, exhibiting novel tunable properties by varying the number of layers [6]. It is well known that monolayers of TMDs such as MoS_2 exhibit a direct bandgap at K point in the Brillouin zone with strong photoluminescence (PL), while multilayers of these materials have an indirect bandgap corresponding to the lowest transition from the valence band maximum (VBM) at the Γ point to the conduction band minimum (CBM) in the Γ–K direction [7]. The indirect nature of multilayers leads to weak PL and thus limits their application in optoelectronic devices such as lasers, but they exhibit higher mobility due to a smaller bandgap and higher density of states, which allow large-scale and high-performance field effect transistors [8].

The properties of TMDs cannot only be tuned by changing thickness, but can also be modulated by strain engineering [9–12], which refers to a general strategy employed in semiconductor manufacturing to enhance device performance. Importantly, monolayer (ML) and few-layer TMD flakes are able to withstand large strains before rupture offering a unique opportunity to introduce large local strains, and are ideal candidates for strain engineering [13]. Recent studies have proved that the optical band gap can be tuned by up to several hundred meV in ML TMD flakes with ultra-large local strains and strain applied to few-layer TMD flakes is able to cause indirect to direct bandgap transitions [14, 15], which greatly extends the application of these materials for optoelectronic devices.

In addition to the tuning ratio of bandgap by strain, another important application of strain engineering is varying the in-plane bandgap profile with inhomogeneous local strain field which is able to control the motion of carriers in semiconducting membranes [16–19]. For example, large-scale quantum-emitter arrays have been created with atomically thin TMDs flakes

Address correspondence to czgu@iphy.ac.cn

such as WSe_2 and WS_2 where point-like strain perturbations modify the bandgap, leading to efficient funneling of excitons towards isolated strain-tuned quantum emitters that exhibit high-purity single photon emission [20, 21]. Furthermore, the recent study has pointed out that there are two possible situations for the motion of photo-generated carriers in 2D materials with inhomogeneous strain [22]. While one possible situation is photo-generated electrons and holes moving towards the same strained region [19–21], another one is electrons and holes migrating towards different strained regions, which is corresponding to a Type-II band alignment built between regions with different strains of 2D materials. Being similar to in-plane 2D heterojunctions [23], this type of gradient bandgap profile of electronic structures induced by local strain will allow new device functionalities, such as in-plane photodetectors and photovoltaic devices, to be integrated within 2D layered materials.

While most previous studies have focused on the local strain effect in ML or bilayer TMDs [11–14], its effect on multilayers has received less attention and rarely has been studied [15, 17]. Comparing to monolayer, multilayer TMDs are more superior and reliable in terms of applicability, because a multiplayer thickness can increase the tenacity of flexible optoelectronic devices and improve carrier mobility [8, 17]. Besides, the stacking symmetry between neighboring layers will break on a multilayer MoS_2 bubble since the deformation is not a constant for the inner layer and outer layer, therefore, some new properties depends on interlayer coupling can be changed in multilayers. In this letter, we used scanning PL and Raman spectroscopies to quantify the local strain over few-layer MoS_2 (3–5 ML) bubbles and demonstrated a continuously varying strain distribution, which gives rise to a gradient direct bandgap profile. And it was found that the unstrained few-layer MoS_2 presents negligible emissions in the corresponding energy range of the appreciable A and B excitons, while the intensity of the A and B excitons becomes a significant increase once the biaxial tensile strain is applied. With the help of the theoretical calculations, we discussed the local strain effect on the direct bandgap emissions of few-layer MoS_2. As an efficient modulation technique, strain engineering is possible to provide a new route for the application of optoelectronic devices using multilayer TMD.

2 Experimental

2.1 Sample fabrication

A MoS_2 crystal (99.999%, HQ Graphene) was used for exfoliation and transfer of atomically thin MoS_2 flakes. Prior to exfoliating MoS_2, the substrate SiO_2/Si is ultrasonically cleaned in acetone, isopropanol, and deionized water, and then loaded into oxygen plasma chamber to further remove ambient adsorbates from its surface, such as water and organic molecules. A fresh surface of MoS_2 after cleaving on tape was brought in contact with the substrate, which is similar to the exfoliation process for preparing graphene. The substrate with the attached tape was annealed in air at 373 K for 2 min using a hot plate. After cooling the sample down to room temperature, the adhesive tape was removed. Heating the substrate has the effect that trapped molecules can partially leak from the edge of MoS_2 flakes and some of them accumulate between few-layer MoS_2 and SiO_2 forming MoS_2 bubbles on the substrate once the MoS_2 flakes covered tape is removed. More detailed discussions about the sample preparation are presented in Fig. S1 in Electronic Supplementary Material (ESM). After sample fabrication, the surface contours of bubbles were characterized by using a Germany Bruker contour GT 3D surface analyzer.

2.2 Optical spectroscopy

A commercial WITec Alpha-SNOM/CRM-200 microscope (Fig. S2 in the ESM) was used to measure PL and Raman maps of the MoS_2 bubbles. The wavelength of excitation laser is 532 nm, the laser power is 1 mW and the spot size of laser is about 800 nm in diameter.

2.3 Density functional theory (DFT) calculations

In our DFT calculations, the generalized gradient approximation (GGA) of Perdew, Burke, and Ernzerhof (PBE) and projector augmented wave (PAW) potentials are used. The kinetic energy cutoff is set to be 350 eV in the plane-wave expansion. A Γ–centered k-point grid of 32 × 32 × 1 is adopted for the Brillouin zone sampling. The criteria of 10^{-6} eV and 0.001 eV/Å for the total energy and Hellman-Feynman force acting on every atom are used in total energy calculation and structural optimization, respectively. Effect of van der Waals (vdW) interaction is accounted for by using empirically-corrected zero-damping DFT-D3 method of Grimme, which is a good description of long-range vdW interactions including those between the packing layers in two-dimensional materials.

3 Results and discussion

A bubble forming by 2D materials has been regarded as a typical model for the investigation of the effect of strain, which has an elastic curved surface and can be stretched up to 20% [14]. In our study, atomically thin MoS_2 flakes were prepared by mechanical exfoliation from a MoS_2 crystal and transferred onto a Si substrate with a 300 nm SiO_2 epi-layer. The thickness of the MoS_2 flakes can be easily identified by color (Fig. 1(a)) [24, 25]. For the formation of bubbles, we have used the same fabrication procedure described in our previous study for graphene bubbles [26]. Comparing to graphene, ML or bilayer MoS_2 bubble is difficult to prepare due to its weaker mechanical properties. Besides, even if we occasionally could get a ML

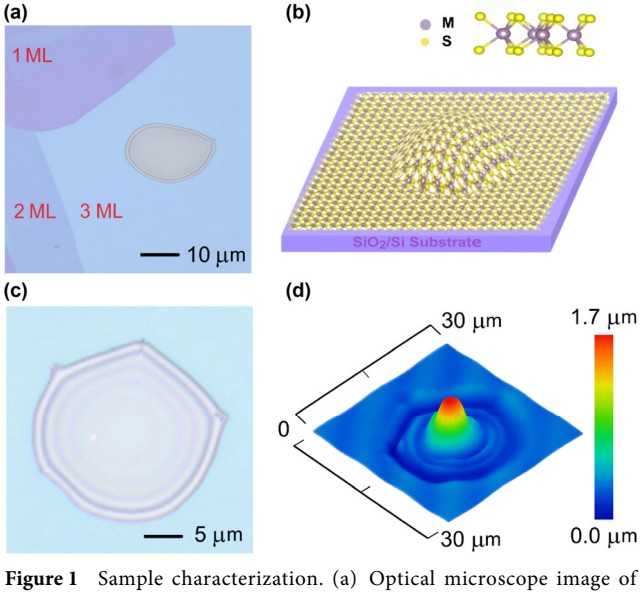

Figure 1 Sample characterization. (a) Optical microscope image of few-layer MoS_2 terraces and bubbles on a Si substrate with a 300 nm SiO_2 epi-layer. (b) Schematic diagram of a MoS_2 bubble with biaxial tensile strain. (c) Optical microscope image of a four-layer MoS_2 bubble. (d) 3D imaging of the bubble measured by a surface analyzer based on the white light interference.

MoS_2 bubble, its diameter would be smaller than 1 μm, which could only result in a weaker strain effect. Figure 1(c) shows the optical micrograph of a typical 4 ML MoS_2 bubble exhibiting an approximately circular shape, where the Newton rings caused by optical interference are well visible. The average radius R of this bubble is about 12.5 μm, and the maximum height h_{max} is 1.6 μm, which are measured by using a surface analyzer based on the white light interference for 3D imaging, as shown in Fig. 1(d). Comparing to other techniques for height profile such as atomic force microscopy (AFM), the 3D surface analyzer has the advantage of non-contact inspection ((Fig. S3 in the ESM)). We evaluate the biaxial tensile strain at the center of this bubble to be about 1%, by using the Hencky's model with a negligible bending stiffness, described by the formula $\varepsilon = \sigma(\nu)(h_{max}/R)^2$, where $\sigma(\nu)$ is a numerical constant that depends only on Poisson's ratio ν [14].

We first studied the effect of strain on few-layer MoS_2 bubbles by scanning PL spectroscopy which has been considered as the standard characterization technique for the strain effect in 2D materials. Although multilayer MoS_2 is an indirect bandgap semiconductor, the PL spectrum of a few-layer MoS_2 bubble with strain presents the obvious emissions from direct bandgap transitions, associated with a weak peak from the indirect transitions (not shown here). As shown in Figs. 2(a) and 2(b), two resonant A and B excitons, corresponding to the photon energies of 1.75 and 1.92 eV, respectively, could be observed on the 4 ML MoS_2 bubble, whereas the unstrained MoS_2 on the substrate exhibits negligible emissions in the corresponding energy range with a low PL intensity (the area outside the bubble), which is similar to the previous observation in wrinkled few-layer MoS_2 flakes [17]. Both PL intensity maps of A and B excitons in Figs. 2(a) and 2(b) show alternating bright and dark rings centered on the tip of the bubble, which could be attributed to the inhomogeneous light excitation on the bubble due to height-dependent interference effect. And the PL intensities are higher at the edge of the MoS_2 bubble and decrease to the center. In order to illustrate the spatial-spectral distribution of A and B excitons, a set of PL spectra from the left edge of the bubble to the center along the horizontal centerline is displayed in Fig. 2(c), which clearly shows redshift of A and B excitons on the bubble. The black curve in Fig. 2(c) is the PL spectrum from the unstrained MoS_2 layer, which exhibits a low PL intensity in the energy range of exciton emissions. And we draw all of the PL spectra along the cutline as the 2D mapping image in Fig. 2(d), where the horizontal axis is the radial coordinate r ranging from −12.5 to 12.5 μm and the vertical axis is the photon energy. Interestingly, the peak positions of A and B excitons show a similar oscillation like as that of intensities, and the exciton energies are higher at the edge and decreases to the center. In other words, the spatial distribution of the peak positions of excitons can be decomposed into two parts: oscillation and gradient change. This type of oscillations has been observed in the Raman maps of graphene bubbles in the previous study [26], which was explained by the optical interference-induced temperature distribution. Such temperature effect is related to the thermal conductivity of materials, and the detailed discussions can be found in Ref. [26]. The observation of the decreasing of the resonant energies of A and B excitons from the edge of the bubble to the center could be attributed to the existence of continuously varying local strain on the MoS_2 bubble [14]. And we measured the maximum redshift of 91 and 59 meV for A and B excitons, respectively (Fig. 3(e)). Another evidence is the decreasing of PL intensities from the edge of the MoS_2 bubble to the center, indicating a continuously varying biaxial strain, which is consistent with previous experiments and theoretical predictions for monolayer and bilayer MoS_2 [14, 27, 28]. As addressed by the theoretical study [28], the decreasing of PL intensity is due to the strong decrease of hole population at K point in the Brillouin zone with increasing strain in the atomically thin MoS_2.

To further verify our argument for continuously varying local strain in few-layer MoS_2 bubbles, we measured corresponding Raman spectra on the same sample. As a fast and nondestructive technique, Raman spectroscopy is a powerful diagnostic tool to investigate the vibrational and physical properties of 2D materials. It has been used to study MoS_2 to determine the number of layers and to quantify strain effect [29–31]. For an unstrained 4 ML MoS_2 flake, the Raman spectrum (the black curve in Fig. 3(c)) shows two characteristic peaks of 383.5 and

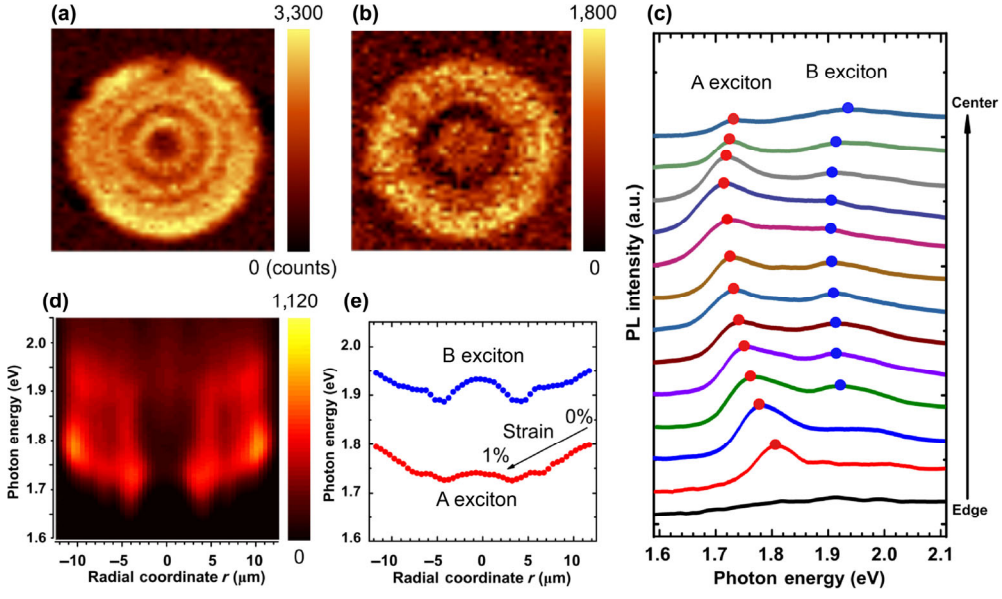

Figure 2 25 μm × 25 μm PL intensity mapping images of a four-layer MoS_2 bubble at the resonant energies of A excitons (a) and B excitons (b). (c) A set of PL spectra from the left edge of the bubble to the center along the horizontal centerline with a distance interval of 1 μm. (d) 2D mapping image of all PL spectra along the horizontal centerline. (d) PL peak positions of A and B excitons as functions of the radial coordinate r over the MoS_2 bubble whose center is defined as $r = 0$.

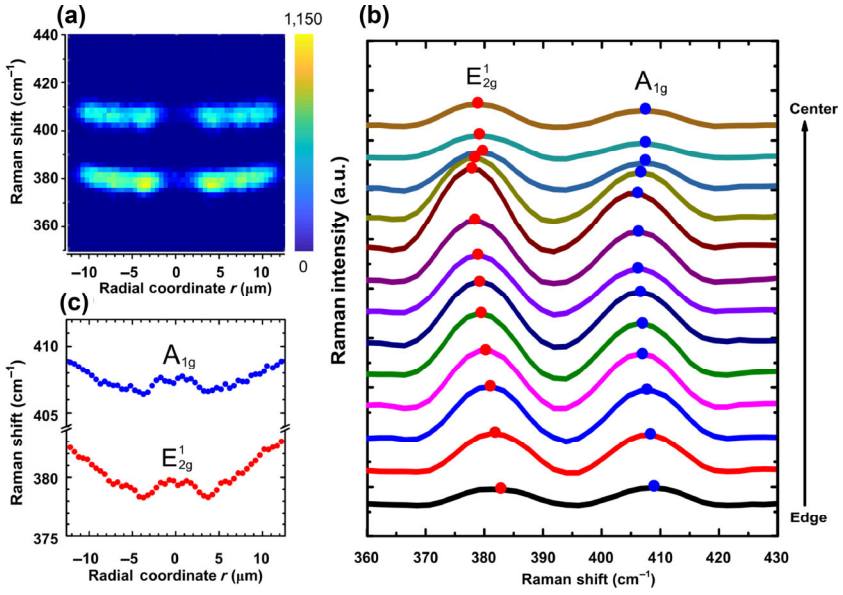

Figure 3 (a) The 2D mapping image of all Raman spectra along the horizontal centerline of the bubble. (b) A set of Raman spectra from the left edge of the bubble to the center along the horizontal centerline with a distance interval of 1 μm. (c) Raman peak positions of both E^1_{2g} and A_{1g} modes as functions of the radial coordinate r over the MoS_2 bubble whose center is defined as $r = 0$.

409.0 cm^{-1}, corresponding to the E^1_{2g} and A_{1g} Raman modes, respectively. The E^1_{2g} is an in-plane vibration mode due to the opposite displacement of the two sulfur atoms with respect to the molybdenum atom while the A_{1g} is an out-of-plane vibration mode of only the sulfur atoms in opposite directions [31]. Figure 3(a) presents the 2D mapping image of Raman spectra along the horizontal centerline of the MoS_2 bubble, which also shows oscillations of the intensities of both E^1_{2g} and A_{1g} modes. In addition to the oscillations, we also saw the continuously softening of both E^1_{2g} and A_{1g} modes from the edge of the MoS_2 bubble to the center, indicating a continuously varying local strain, and measured the mode shift of −5.2 cm^{-1} for the E^1_{2g} and −2.5 cm^{-1} for the A_{1g}, respectively (Figs. 3(b) and 3(c))). By using the formula $\gamma = (\omega - \omega_0)/(2\omega_0)$ (ω and ω_0 are the Raman frequencies at finite strain and zero strain, respectively), we calculate the Grüneisen parameters to be γ_1 = 0.45 for E^1_{2g} mode and γ_2 = 0.21 for A_{1g} mode, which is close to the result of previous experimental studies [14]. The Grüneisen parameters describe the effect of changing the volume of a crystal lattice on its vibrational properties and also determine the thermomechanical properties [32]. Moreover, it was found that the Raman oscillations in MoS_2 bubbles are not as obvious as graphene due to a smaller temperature coefficient [26]. And we estimate the temperature difference resulting in the oscillations to be ~ 200 K around the center, using the formula $\omega(T) = \omega(T_0) + \chi\Delta T$ [33], where χ is the first-order temperature coefficient of MoS_2.

In order to further understand our experimental results, especially the effects of tensile strain on the tuning of the electronic and vibrational properties of few-layer MoS_2, we performed *ab initio* simulations which are based on DFT and implemented by the VASP package [34, 35]. The few-layer MoS_2 is mimicked by a slab model consisting 2–5 layers of single-layer MoS_2 which has hexagonal symmetry, and a vacuum region of about 16 Å along the direction normal to the few-layer surface is set to avoid interaction between two adjacent periodic images (Fig. S4 in the ESM). It is well-known that the inter-layer packing structure of the bulk MoS_2 is AB-stacking: the neighboring layers are aligned, and one type of atom is on top of the other type. A theoretical study showed that the lowest-energy packing structure of the bilayer MoS_2 is also the AB stacking, but its binding energy is very close to that of the AC-stacking in which the S and Mo atoms of the top layer are on top of the Mo atoms and hexagon centers of the bottom layer, respectively [36]. So we have considered these two packing structures in the structural optimizations, and the calculation results show that for the bilayer, tri-layer and five-layer MoS_2, the AB-stacking is indeed the lowest-energy packing structure, but the four-layer MoS_2 prefers to be the AC-stacking, although the energy differences are very small (see Table S1 in the ESM).

Figure 4(a) shows the band structure of the four-layer MoS_2, from which one can find that the four-layer MoS_2 is a semiconductor with indirect bandgap, in agreement with previous studies showing that MoS_2 turns from the direct bandgap semiconductor to the indirect bandgap semiconductor when the layers number is larger than one [7]. Although the bandgap of the whole system is indirect, the few-layer MoS_2 had been found to still possess appreciable PL intensity, i.e., A and B excitons we observed, which was ascribed to the direct transition at K point of the Brillouin zone due to the presence of hot carriers that transiently occupy states near the K-point before fully relaxing [7, 37]. Here we denote the bandgap at the K point as E_g (K). The change of this bandgap of the few-layer MoS_2 with the in-plane biaxial tensile strain ε is shown in Fig. 4(b). It displays the almost linear relationship between the ΔE_g (K) and the strain ε, consistent with previous studies [37, 38]. And it is also noted that the layers number from 2 to 5 has little influence on the ΔE_g (K)−ε curve, except for a smaller deviation of the four-layer MoS_2 because of the difference of their packing structures. But the qualitative features of band structure are less affected by this difference of the packing structure, as suggested by the band structures of 2–5 ML MoS_2 in Fig. S4 in the ESM. Our result shows that the biaxial strain-induced energy shift of E_g (K) is about −107 meV% for the bilayer, trilayer and five-layer, and about −114 meV% for the four-layer, close to the previous calculation (−113 meV% for the bilayer MoS_2) [38]. On the other hand, our calculation shows the vibrational wavenumbers of both the E^1_{2g} and A_{1g} modes of the four-layer MoS_2 have also almost linear relationships with the biaxial tensile strain, and their corresponding shift rates are −4.9 cm^{-1}% and −1.5 cm^{-1}%, respectively. These theoretical results are close to the

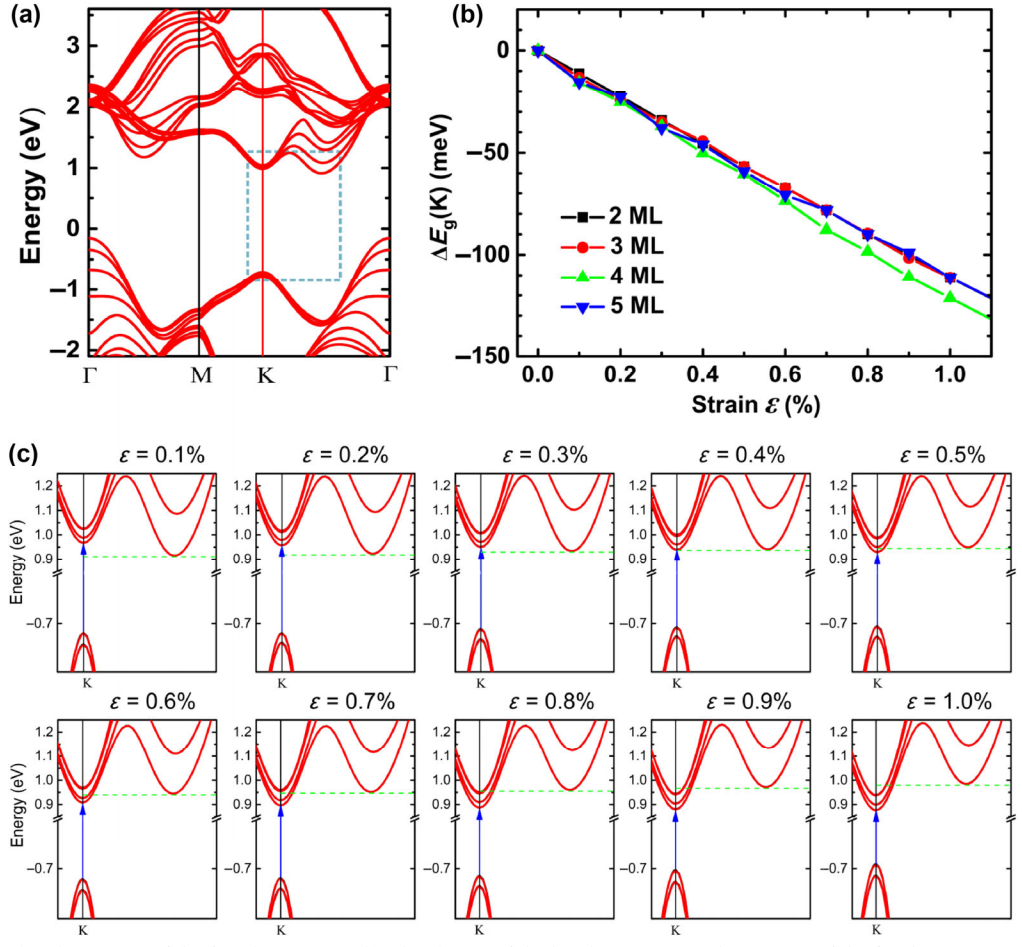

Figure 4 (a) The band structure of the four-layer MoS_2. (b) The change of the bandgap E_g (K) at the K point of the few-layer (2–5 ML) MoS_2 with the in-plane biaxial tensile strain ε. (c) The band structures magnified around the K point of the four-layer MoS_2 with different biaxial tensile strains. The green dash line indicates the energy of local band minimum at a specific k-point along the Γ–K direction. The Fermi level is set to zero for all figures of band structures.

corresponding experimental values of our measurements.

An interesting phenomenon is that the unstrained MoS_2 presents negligible emissions in the corresponding energy range of the appreciable A and B excitons observed in the MoS_2 sample with the biaxial tensile strain in Fig. 2(c), which suggests a significant increase of the intensity of the A and B excitons once the biaxial tensile strain is applied. The funnel effect was previously thought to be responsible for this PL enhancement, but the PL enhancement induced by the funnel effect is commonly about twice for the MoS_2 materials [19], not enough to interpret the significant increase of PL intensity in our experiment. It can be understood by our theoretical calculations as follows. Figure 4(c) shows the band structures magnified around the K point of the four-layer MoS_2 with different biaxial tensile strains. It is found that the CBM for the unstrained four-layer MoS_2 is not at the K point, but at a specific k-point along the Γ–K direction, with an eigen-energy difference of 0.07 eV. In fact, this is also a characteristic of the bulk MoS_2. However, if the biaxial tensile strain is applied and larger than 0.3%, the CBM will transfer to the K point. The eigen-energy difference between the K point and that specific k-point of the conductive band turns to −0.04 eV for the four-layer MoS_2 with the biaxial strain of 0.6%, and reaches to −0.11 eV when the biaxial strain is 1.0%. This change makes the bandgap at the K point more "direct" and then the K-valley can accommodate higher carrier densities before the another valley is populated, which will bring a significant enhancement of the direct transition at K point (A and B excitons). A theoretical study predicted the PL enhancement by an order of magnitude for slight tensile strain of the monolayer MoS_2 [28], in which the mechanism is very similar to that in our study.

At last, it is worth to talk more about the origin of the continuously varying local strain in bubbles forming by 2D materials. In the previous theoretical study [39], Fichter had pointed the problem of the Hencky's classic solution for the large deflections of a clamped, circular isotropic membrane under uniform pressure, which gives rise to a homogeneous biaxial strain over the membrane. This classic solution is observed actually to be for uniform lateral loading because the radial component of the pressure acting on the deformed membrane is neglected. Fichter's calculations show that the deflection differences for uniform lateral loading (Hencky's problem) and uniform-pressure loading are very small for $q = h_{max}/R = 0.01$, whereas a basic difference between deflection shapes becomes quit apparent for $q = 0.1$ with the effect on lateral deflection of retaining the radial components of the pressure which could induce radial local in-plane strain. Furthermore, in the recent study of Raman spectra from unsupported monolayer graphene under pressure [40], the authors have estimated the out-of-plane strain and stiffness for 2D materials and indicated that the very soft out-of-plane stiffness of graphene is responsible for the sub-linearity in the shift of the in-plane phonon frequency with pressure. Their results mean that 3D elastic stiffness tensor does retain meaning and can be ascribed to 2D materials. As to this regard, the additional theoretical and experimental efforts, therefore, will

need to be carried out in order to understand local strain in 2D materials.

4 Conclusions

In summary, we used scanning PL and Raman spectroscopies to investigate the local strain distribution over few-layer MoS_2 bubbles. The observations of continuous shifts of both resonant exciton energies and vibrational modes indicate the existence of continuously varying local tensile strain on MoS_2 bubbles. We measured the tuning ratio of the bandgap and Raman modes by strain in MoS_2 bubbles. These findings are corroborated by our theoretical simulations based on DFT. The gradient profile of electronic structures in these few-layer MoS_2 bubbles induced by local strain is similar to that of in-plane TMD heterojunctions, which will allow new device functionalities, such as in-plane photodetectors and photovoltaic devices, to be integrated within 2D layered materials, but local strain provides a convenient way to realize them without any chemical modification and additional composition.

Acknowledgements

This work was financially supported by the National Key Research and Development Program of China (Nos. 2016YFA0200400, 2016YFA0200800, 2016YFA0200603, 2017YFA0204904, 2019YFA0308000, and 2018YFA0704200), the National Natural Science Foundation of China (Nos. 61888102, 11574369, 11674387, 11574368, 11574385, and 11874405), the Key Research Program of Frontier Sciences of CAS (No. QYZDJ-SSWSLH042), and the Youth Innovation Promotion Association of CAS (No. 2019007). B. L. thanks the Supercomputing Center at USTC, Supercomputing Center of Chinese Academy of Sciences in Tianjin, and Shanghai Supercomputer Center for providing the computing resources.

Electronic Supplementary Material: Supplementary material (further details of the formation of MoS_2 bubbles, experimental instruments, theoretical calculations and additional data) is available in the online version of this article at https://doi.org/10.1007/s12274-020-2809-6.

References

[1] Novoselov, K. S.; Jiang, D.; Schedin, F.; Booth, T. J.; Khotkevich, W. S.; Morozov, V.; Geim, A. K. Two-dimensional atomic crystals. *Proc. Natl. Acad. Sci. USA* **2005**, *102*, 10451–10453.

[2] Butler, S. Z.; Hollen, S. M.; Cao, L. Y.; Cui, Y.; Gupta, J. A.; Gutiérrez, H. R.; Heinz, T. F.; Hong, S. S.; Huang, J. X.; Ismach, A. F. et al. Progress, challenges, and opportunities in two-dimensional materials beyond graphene. *ACS Nano* **2013**, *7*, 2898–2926.

[3] Manzeli, S.; Ovchinnikov, D.; Pasquier, D.; Yazyev, O. V.; Kis, A. 2D transition metal dichalcogenides. *Nat. Rev. Mater.* **2017**, *2*, 17033.

[4] Mak, K. F.; Xiao, D.; Shan, J. Light–valley interactions in 2D semiconductors. *Nat. Photonics* **2018**, *12*, 451–460.

[5] Mak, K. F.; Shan, J. Photonics and optoelectronics of 2D semiconductor transition metal dichalcogenides. *Nat. Photonics* **2016**, *10*, 216–226.

[6] Wang, H. T.; Yuan, H. T.; Hong, S. S.; Li, Y. B.; Cui, Y. Physical and chemical tuning of two-dimensional transition metal dichalcogenides. *Chem. Soc. Rev.* **2015**, *44*, 2664–2680.

[7] Wang, G.; Chernikov, A.; Glazov, M. M.; Heinz, T. F.; Marie, X.; Amand, T.; Urbaszek, B. *Colloquium*: Excitons in atomically thin transition metal dichalcogenides. *Rev. Mod. Phys.* **2018**, *90*, 021001.

[8] Kim, S.; Konar, A.; Hwang, W. S.; Lee, J. H.; Lee, J.; Yang, J.; Jung, C.; Kim, H.; Yoo, J. B.; Choi, J. Y. et al. High-mobility and low-power thin-film transistors based on multilayer MoS_2 crystals. *Nat. Commun.* **2012**, *3*, 1011.

[9] Xie, S. E.; Tu, L. J.; Han, Y. M.; Huang, L. J.; Kang, K.; Lao, K. U.; Poddar, P.; Park, C.; Muller, D. A.; DiStasio, R. A. Jr. et al. Coherent, atomically thin transition-metal dichalcogenide superlattices with engineered strain. *Science* **2018**, *359*, 1131–1136.

[10] Martella, C.; Mennucci, C.; Lamperti, A.; Cappelluti, E.; de Mongeot, F. B.; Molle, A. Designer shape anisotropy on transition-metal -dichalcogenide nanosheets. *Adv. Mater.* **2018**, *30*, 1705615.

[11] Zhao, X. X.; Ding, Z. J.; Chen, J. Y.; Dan, J. D.; Poh, S. M.; Fu, W.; Pennycook, S. J.; Zhou, W.; Loh, K. P. Strain modulation by van der Waals coupling in bilayer transition metal dichalcogenide. *ACS Nano* **2018**, *12*, 1940–1948.

[12] Ahn, G. H.; Amani, M.; Rasool, H.; Lien, D. H.; Mastandrea, J. P.; Ager III, J. W. Dubey, M.; Chrzan, D. C.; Minor, A. M.; Javey, A. Strain-engineered growth of two-dimensional materials. *Nat. Commun.* **2017**, *8*, 608.

[13] Bertolazzi, S.; Brivio, J.; Kis, A. Stretching and breaking of ultrathin MoS_2. *ACS Nano* **2011**, *5*, 9703–9709.

[14] Lloyd, D.; Liu, X. H.; Christopher, J. W.; Cantley, L.; Wadehra, A.; Kim, B. L.; Goldberg, B. B.; Swan, A. K.; Bunch, J. S.; Scott, J. Band gap engineering with ultralarge biaxial strains in suspended monolayer MoS_2. *Nano Lett.* **2016**, *16*, 5836–5841.

[15] Desai, S. B.; Seol, G.; Kang, J. S.; Fang, H.; Battaglia, C.; Kapadia, R.; Ager, J. W.; Guo, J.; Javey, A. Strain-induced indirect to direct bandgap transition in multilayer WSe_2. *Nano Lett.* **2014**, *14*, 4592–4597.

[16] Franzl, T.; Klar, T. A.; Schietinger, S.; Rogach, A. L.; Feldmann, J. Exciton recycling in graded gap nanocrystal structures. *Nano Lett.* **2004**, *4*, 1599–1603.

[17] Castellanos-Gomez, A.; Roldán, R.; Cappelluti, E.; Buscema, M.; Guinea, F.; van der Zant, H. S. J.; Steele, G. A. Local strain engineering in atomically thin MoS_2. *Nano Lett.* **2013**, *13*, 5361–5366.

[18] Feng, J.; Qian, X. F.; Huang, C. W.; Li, J. Strain-engineered artificial atom as a broad-spectrum solar energy funnel. *Nat. Photonics* **2012**, *6*, 866–872.

[19] Li, H.; Contryman, A. W.; Qian, X. F.; Ardakani, S. M.; Gong, Y. J.; Wang, X. L.; Weisse, J. M.; Lee, C. H.; Zhao, J. H.; Ajayan, P. M. et al. Optoelectronic crystal of artificial atoms in strain-textured molybdenum disulphide. *Nat. Commun.* **2015**, *6*, 7381.

[20] Branny, A.; Kumar, S.; Proux, R.; Gerardot, B. D. Deterministic strain-induced arrays of quantum emitters in a two-dimensional semiconductor. *Nat. Commun.* **2017**, *8*, 15053.

[21] Palacios-Berraquero, C.; Kara, D. M.; Montblanch, A. R. P.; Barbone, M.; Latawiec, P.; Yoon, D.; Ott, A. K.; Loncar, M.; Ferrari, A. C.; Atatüre, M. Large-scale quantum-emitter arrays in atomically thin semiconductors. *Nat. Commun.* **2017**, *8*, 15093.

[22] Sun, J. Y.; Li, X. X.; Yang, J. L. Significantly enhanced charge separation in rippled monolayer graphitic C_3N_4. *ChemCatChem* **2019**, *11*, 6252–6257.

[23] Zhang, C. D.; Li, M. Y.; Tersoff, J.; Han, Y. M.; Su, Y. S.; Li, L. J.; Muller, D. A.; Shih, C. K. Strain distributions and their influence on electronic structures of WSe_2–MoS_2 laterally strained heterojunctions. *Nat. Nanotechnol.* **2018**, *13*, 152–158.

[24] Blake, P.; Hill, E. W.; Castro Neto, A. H.; Novoselov, K. S.; Jiang, D.; Yang, R.; Booth, T. J.; Geim, A. K. Making graphene visible. *Appl. Phys. Lett.* **2007**, *91*, 063124.

[25] Castellanos-Gomez, A.; Agraït, N.; Rubio-Bollinger, G. Optical identification of atomically thin dichalcogenide crystals. *Appl. Phys. Lett.* **2010**, *96*, 213116.

[26] Huang, Y.; Wang, X.; Zhang, X.; Chen, X. J.; Li, B. W.; Wang, B.; Huang, M.; Zhu, C. Y.; Zhang, X. W.; Bacsa, W. S. et al. Raman spectral band oscillations in large graphene bubbles. *Phys. Rev. Lett.* **2018**, *120*, 186104.

[27] Conley, H. J.; Wang, B.; Ziegler, J. I.; Haglund, R. F. Jr.; Pantelides, S. T.; Bolotin, K. I. Bandgap engineering of strained monolayer and bilayer MoS_2. *Nano Lett.* **2013**, *13*, 3626–3630.

[28] Steinhoff, A.; Kim, J. H.; Jahnke, F.; Rösner, M.; Kim, D. S.; Lee, C.; Han, G. H.; Jeong, M. S.; Wehling, T. O.; Gies, C. Efficient excitonic photoluminescence in direct and indirect band gap monolayer MoS_2. *Nano Lett.* **2015**, *15*, 6841–6847.

[29] Li, H.; Zhang, Q.; Yap, C. C. R.; Tay, B. K.; Edwin, T. H. T.; Olivier, A.; Baillargeat, D. From bulk to monolayer MoS_2: Evolution of Raman scattering. *Adv. Funct. Mater.* **2012**, *22*, 1385–1390.

[30] Wang, Y. L.; Cong, C. X.; Qiu, C. Y.; Yu, T. Raman spectroscopy study

of lattice vibration and crystallographic orientation of monolayer MoS_2 under uniaxial strain. *Small* **2013**, *9*, 2857–2861.

[31] Nayak, A. P.; Pandey, T.; Voiry, D.; Liu, J.; Moran, S. T.; Sharma, A.; Tan, C.; Chen, C. H.; Li, L. J.; Chhowalla, M. et al. Pressure-dependent optical and vibrational properties of monolayer molybdenum disulfide. *Nano Lett*. **2015**, *15*, 346–353.

[32] Zabel, J.; Nair, R. R.; Ott, A.; Georgiou, T.; Geim, A. K.; Novoselov, K. S.; Casiraghi, C. Raman spectroscopy of graphene and bilayer under biaxial strain: Bubbles and balloons. *Nano Lett*. **2012**, *12*, 617–621.

[33] Hu, Z. J.; Bao, Y. J.; Li, Z. W.; Gong, Y. J.; Feng, R.; Xiao, Y. D.; Wu, X. C.; Zhang, Z. H.; Zhu, X.; Ajayan, P. M. et al. Temperature dependent Raman and photoluminescence of vertical WS_2/MoS_2 monolayer heterostructures. *Sci*. *Bull*. **2017**, *62*, 16–21.

[34] Kresse, G.; Furthmüller, J. Efficiency of *ab-initio* total energy calculations for metals and semiconductors using a plane-wave basis set. *Comput*. *Mater*. *Sci*. **1996**, *6*, 15–50.

[35] Kresse, G.; Furthmüller, J. Efficient iterative schemes for *ab initio* total-energy calculations using a plane-wave basis set. *Phys*. *Rev*. *B* **1996**, *54*, 11169–11186.

[36] Liu, Q. H.; Li, L. Z.; Li, Y. F.; Gao, Z. X.; Chen, Z. F.; Lu, J. J. Tuning electronic structure of bilayer MoS_2 by vertical electric field: A First-Principles investigation. *Phys*. *Chem*. *C* **2012**, *116*, 21556–21562.

[37] McCreary, A.; Ghosh, R.; Amani, M.; Wang, J.; Duerloo, K. A. N.; Sharma, A.; Jarvis, K.; Reed, E. J.; Dongare, A. M.; Banerjee, S. K. et al. Effects of uniaxial and biaxial strain on few-layered terrace structures of MoS_2 grown by vapor transport. *ACS Nano* **2016**, *10*, 3186–3197.

[38] Dong, L.; Dongare, A. M.; Namburu, R. R.; O'Regan, T. P.; Dubey, M. Theoretical study on strain induced variations in electronic properties of 2H–MoS_2 bilayer sheets. *Appl*. *Phys*. *Lett*. **2014**, *104*, 053107.

[39] Fichter, W. B. Some solutions for the large deflections of uniformly loaded circular membranes. *NASA Tech. Pap*. **1997**, *3658*, 1–20.

[40] Sun, Y. W.; Liu, W.; Hernandez, I.; Gonzalez, J.; Rodriguez, F.; Dunstan, D. J.; Humphreys, C. J. 3D strain in 2D materials: To what extent is monolayer graphene graphite? *Phys*. *Rev*. *Lett*. **2019**, *123*, 135501.